Compact High-T_c Superconducting Terahertz emitter operating up to 86 K

Hancong Sun,[1] Raphael Wieland,[2] Zuyu Xu,[1] Zaidong Qi,[1] Yangyang Lv,[1] Ya Huang,[1] Huili Zhang,[1] Xianjing Zhou,[1] Jun Li,[1] Yonglei Wang,[1] Fabian Rudau,[2] Johannes S. Hampp,[2] Dieter Koelle,[2] Shigeyuki Ishida,[3] Hiroshi Eisaki,[3] Yoshiyuki Yoshida,[3] Biaobing Jin,[1] Valery P. Koshelets,[4] Reinhold Kleiner,[2] Huabing Wang,[1,*] and Peiheng Wu[1]

[1]*Research Institute of Superconductor Electronics, Nanjing University, Nanjing 210023, China*

[2]*Physikalisches Institut and Center for Quantum Science in LISA$^+$, Universität Tübingen, 72076 Tübingen, Germany*

[3]*Electronics and Photonics Research Institute, Advanced Industrial Science and Technology, Tsukuba 3058568, Japan*

[4]*Kotel'nikov Institute of Radio Engineering and Electronics, Moscow 125009, Russia*

We report on a Stirling-cooled compact $Bi_2Sr_2CaCu_2O_{8+\delta}$ intrinsic Josephson-junction stack with very high critical current density and improved cooling, operating at bath temperatures T_b up to 86 K. The square stand-alone stack is embedded between two sapphire substrates. For bath temperatures between 27.8 and 86 K emission is observed at frequencies from 0.356 to 2.09 THz. The emission power exceeds 1 μW at bath temperatures between 60 and 80 K for emission frequencies between 0.5 and 0.88 THz. A record high value of 0.577 THz is obtained for the emission frequency at $T_b = 80$ K, which is important for potential applications using liquid nitrogen as a coolant. We also compare our experimental results with numerical simulations based on three-dimensional coupled sine-Gordon equations combined with heat diffusion equations.

I. INTRODUCTION

Terahertz (THz) emitters are investigated intensively due to their potential applications in high-bandwidth communication, public security, environmental monitoring, etc. [1,2]. As compact solid-state devices, intrinsic Josephson-junction (IJJ) stacks made of the high-critical-temperature (T_c) superconductor $Bi_2Sr_2CaCu_2O_{8+\delta}$ (BSCCO) have attracted much attention due to their potential to radiate especially at subterahertz frequencies [3–5], and intensive experimental [6–38] and theoretical [39–64] research has been performed. The possibility to perform terahertz imaging [65–68] and gas detection [69] or to realize an all-high-T_c integrated receiver [70] has been demonstrated.

In BSCCO, terahertz radiation is generated by the ac Josephson effect. A suitably patterned single crystal of 1-μm thickness forms a stack of $N \sim 670$ IJJs. If the voltage across all IJJs is equal, the junctions oscillate at a frequency $f_J = V/N\Phi_0$ (0.4836 THz/mV per junction), where Φ_0 is the flux quantum and V is the voltage across the stack. To obtain a high emission power P_e the IJJs in the stack should be synchronized. Coherent off-chip

terahertz emission was first demonstrated for 1-μm-thick BSCCO stacks, with an extrapolated output power of up to 0.5 μW for emission frequencies f_e between 0.5 and 0.85 THz [6], and it has been proposed that resonant modes utilizing the stack as a cavity and oscillating along the width of the stack play an important role for synchronization. A variety of cavity resonances have indeed been found and analyzed [7–9,11,13,14,47,62–64]. For the best stacks the detected terahertz power is now on the order of tens of microwatts [22,23,27,70], with a maximum value of 610 μW achieved by a synchronized three-mesa array [22]. For typical stacks with lateral sizes in the 100-μm range the emission frequency ranges from 0.2 to 2.4 THz [25–27,35]. Further, it has been shown recently that also smaller stacks can emit radiation between 1 and 11 THz [37].

The large BSCCO stacks are subject to strong Joule heating. Since the out-of-plane resistivity of this material decreases with increasing temperature, the current-voltage characteristics (IVCs) exhibit a positive differential resistance at low currents but start to back-bend at larger currents and the differential resistance becomes negative. Above some current in the back-bending region, the current and temperature distribution in the stack become strongly nonuniform and a hot spot (i.e., a region with a

---

*hbwang@nju.edu.cn

024041-1

temperature above T_c) forms [8,11,19,21,38,50,57]. The hot spot can coexist with regions that are still superconducting, producing terahertz radiation. The hot spot also affects the properties of the terahertz radiation. For example, one observes a much lower linewidth of radiation in the presence of the hot spot [18], and it can be helpful to tune the frequency range of emission [28,31,71]. On the other hand, Joule heating and, in particular, the formation of the hot spot limits the maximum voltage across the stack and thus the emission frequency.

Over time, to improve the thermal and electromagnetic properties of IJJ stacks, gold-BSCCO-gold (GBG) stand-alone stacks were fabricated instead of conventional mesas patterned on a thick BSCCO base crystal, which has poor thermal conductivity perpendicular to the layers (c direction) [17,70]. Subsequently, stacks sandwiched between two thermally-well-conducting substrates were created for a more efficient heat exhaust, and the highest emission frequency was increased gradually [25–27]. In addition, Tsujimoto *et al.* [32] observed an increase of the maximum emission frequency for Pb-doped BSCCO stacks and argued that the higher interlayer critical current density j_c leads to an increase of the Josephson plasma frequency, which most likely determines the cutoff frequency of emission. However, for high operating temperatures above 70 K, the reported BSCCO terahertz emitters always either have no emission or radiate at a frequency well below 500 GHz [25–27,29,35], limiting their applicability.

To improve the emission properties especially at high operating temperatures, we fabricate a stand-alone stack from a slightly overdoped (rather than the typically used slightly underdoped) BSCCO crystal with higher T_c of approximately 91.5 K and j_c (4.2 K) of approximately 2 kA/cm^2, and then embed it in a sandwich structure for efficient heat exhaust. The transport and emission characteristics are studied at different bath temperatures T_b from 27.8 to 86 K, with a tunable emission-frequency range from 0.356 to 2.09 THz. A record high 0.577-THz emission peak frequency is observed at $T_b = 80$ K.

II. SAMPLE PREPARATION AND MEASUREMENT TECHNIQUES

The IJJ stack is fabricated from a slightly overdoped BSCCO single crystal grown by a floating-zone technique, with a transition temperature T_c of 91.5 K. To form the stack, a 100-nm-thick gold layer is deposited on the surface of the crystal immediately after cleavage by dual-adhesive tape. The sample is then turned over and the gold-covered side is glued onto the surface of a sapphire substrate by polyimide. Next, the upper surface of the crystal is cleaved by tape, and a 100-nm-thick gold film acting as the top electrode is evaporated on the fresh crystal surface. By photolithography a 200×200 μm^2 square is patterned on the gold film. Most parts of the GBG structure are removed
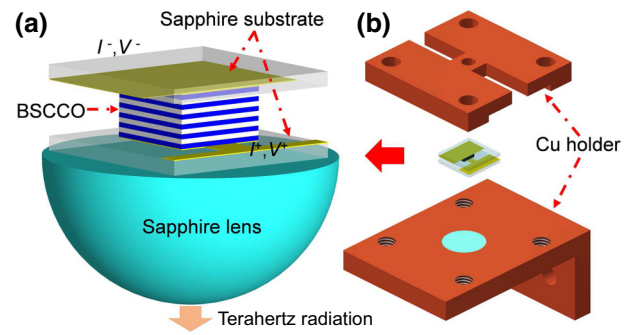

FIG. 1. (a) The BSCCO stack sandwiched between two sapphire substrates and mounted on a hemispheric sapphire lens. Current and voltage leads are indicated. (b) The Cu holders used to fix and cool the BSCCO stack (not to scale).

by ion milling, except for the parts underneath the protected square and the bottom gold film. The BSCCO part of the structure has a thickness of about 900 nm, corresponding to approximately 600 IJJs. To pattern the bottom electrode, photoresist touching the square is pasted manually onto the bottom gold film and subsequently the unprotected bottom gold parts are removed by ion milling. After removal of the photoresist, the sapphire substrate hosting the BSCCO emitter (200×200 μm^2 wide) is glued onto a hemispheric sapphire lens having a diameter of 6.0 mm. Then another sapphire substrate, with one side covered with a 100-nm-thick gold layer, is placed on the top surface of the IJJ stack to contact the top electrode, as shown in Fig. 1(a). Finally, the assembled sandwich structure is fixed between two Cu holders [see Fig. 1(b)] and placed into a Stirling cryocooler (RICOR K535), which can cool down to 27.8 K from room temperature. The lateral size of the Cu holder is 30×20 mm^2, and the overall size of the device, including the cryocooler, is about $41 \times 35 \times 21$ cm^3. The terahertz radiation emitted from the IJJ stacks is modulated by a mechanical chopper with a modulation frequency of 102 Hz and then detected by a Si bolometer. A homemade terahertz interferometer with a resolution of about 15 GHz is used to measure the terahertz-radiation frequency [72].

III. RESULTS

Figure 2(a) displays the out-of-plane resistance R of the stack vs bath temperature T_b. Below T_c there is a contact resistance of about 4 Ω, which amounts to almost half of the sample resistance near T_c. Above T_c the contact resistance may be temperature dependent, giving uncertainties in estimating the doping state of the crystal from the shape of R vs T_b. However, the fact that R vs T_b decreases with decreasing temperature down to about 120 K indicates that the crystal is indeed slightly overdoped, perhaps with δ around 0.26 [73,74].

Figure 2(b) shows the outermost branch of the IVCs at the four bath temperatures $T_b = 27.8, 60, 70,$ and 85 K.
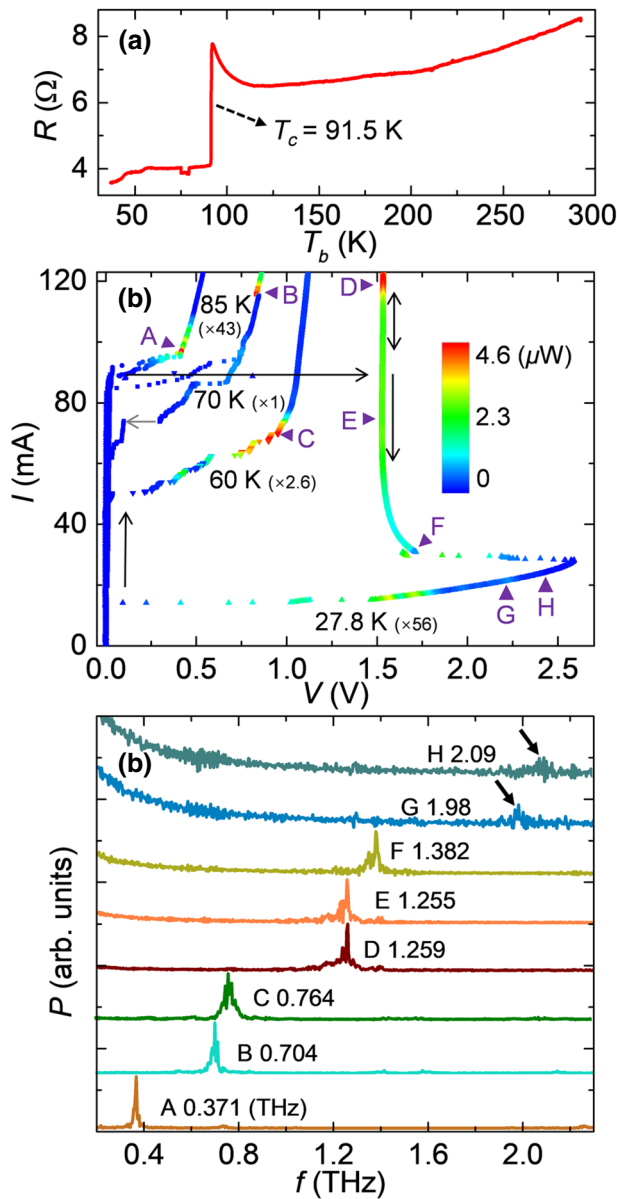
FIG. 2. (a) Out-of-plane resistance of the BSCCO stack vs bath temperature. (b) IVCs for four bath temperatures. The corresponding terahertz-emission power is indicated by colors. The emission power of the 85, 60, and 27.8-K curves is multiplied by factors of 43, 2.6, and 56, respectively, to match the color scale. For the 27.8-K curve black arrows indicate the sweep direction, and for the 70-K curve a gray arrow marks a voltage jump. (c) Fourier spectra of the emitted radiation for the bias points A–H indicated in (b). Adjacent curves are vertically offset for clarity, and the frequency values of the highest emission peak, defining f_e, are indicated for each curve.

The contact resistance is subtracted. For each curve the current is ramped from 0 up to 120 mA and then decreased back to zero. The IVCs exhibit a positive differential resistance in the voltage state at $T_b = 60$, 70, and 85 K. At $T_b = 27.8$ K the IVC exhibits strong back-bending,

indicating the presence of a hot spot for bias currents larger than 28 mA. At $T_b = 27.8$ K the highest voltage across the stack is 2.593 V (about 4.32 mV for each Josephson junction), indicating the efficient cooling of this device. When the current is *increased* from zero, for $T_b = 27.8$, 60, and 85 K the stack switches from the zero-voltage state to the resistive state at a current of about 89 mA. For $T_b = 70$ K the switching current is slightly lower, about 85 mA. The corresponding current densities are about 220 A/cm^2. Although this value is higher than switching current densities reported earlier [25,28,32,69,70] the fact that the switching current is nearly temperature independent over a large range of bath temperatures suggests that the actual critical current I_c and the corresponding current density j_c must be much higher. For slightly overdoped samples, measurements on small IJJ stacks revealed j_c of at least 2 kA/cm^2 at 4.2 K, which would correspond to a critical current of 0.8 A for our stack [75]. The low value of the observed switching current may arise from the nucleation of some Josephson vortices, immediately switching the whole stack into its resistive state. Such a scenario is not unrealistic, since our stack is much larger than the Josephson length, which is about 0.3 μm for $j_c = 2$ kA/cm^2 [60,61].

The terahertz-emission power, as detected by the Si bolometer, is indicated by the colors in Fig. 2(b). Even at the very high bath temperature of 85 K the device emits radiation, with a maximum emission power of 107 nW at bias point A in Fig. 2(b). Here, the emission frequency is 0.371 THz [see Fig. 2(c)]. The highest emission power of the stack occurs at $T_b = 70$ K, at $I = 117.5$ mA and $V = 0.865$ V, and amounts to about 4.6 μW, with a measured emission frequency $f_e = 0.704$ THz. For $T_b = 60$ K the maximum emission power is 1.7 μW, at an emission frequency of 0.764 THz. At $T_b = 27.8$ K terahertz emission is observed in both the high-bias region and the low-bias region. In the high-bias region, the stack has stable terahertz emission over a wide current range from 29.5 to 120 mA, covering a voltage range from 1.530 to 1.718 V and a frequency range from 1.255 to 1.382 THz. The maximum emission power is about 74.8 nW at $I = 119.3$ mA [point D in Figs. 2(b) and 2(c)], with an emission frequency $f_e = 1.259$ THz. For frequencies above 1.38 THz [bias point F in Figs. 2(b) and 2(c)] the emission power strongly decreases; however, some signal is still present there, as indicated by the spectra at bias points G and H located in the low-bias region [see Figs. 2(b) and 2(c)]. The emission power detected at these points is 12 and 6.6 nW, respectively. The highest recordable emission frequency is around 2.09 THz and appears at bias point H, at current $I = 25.09$ mA and voltage $V = 2.48$ V.

Figure 3 shows more detailed data for a bath temperature of 80 K (i.e., slightly above liquid-nitrogen temperature). When the current is increased from zero, the stack switches
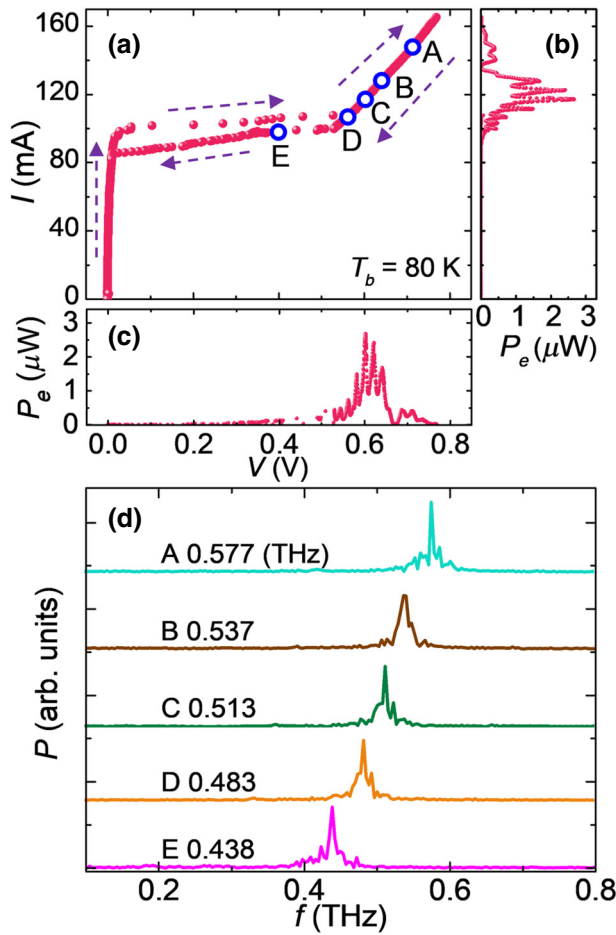
FIG. 3. (a) IVC of the emitter, as measured at $T_b = 80$ K. Arrows indicate the sweep direction. (b),(c) The emission power as a function of I and V, respectively. (d) Fourier spectra of the emitted radiation for bias points *A–E* indicated in (a).
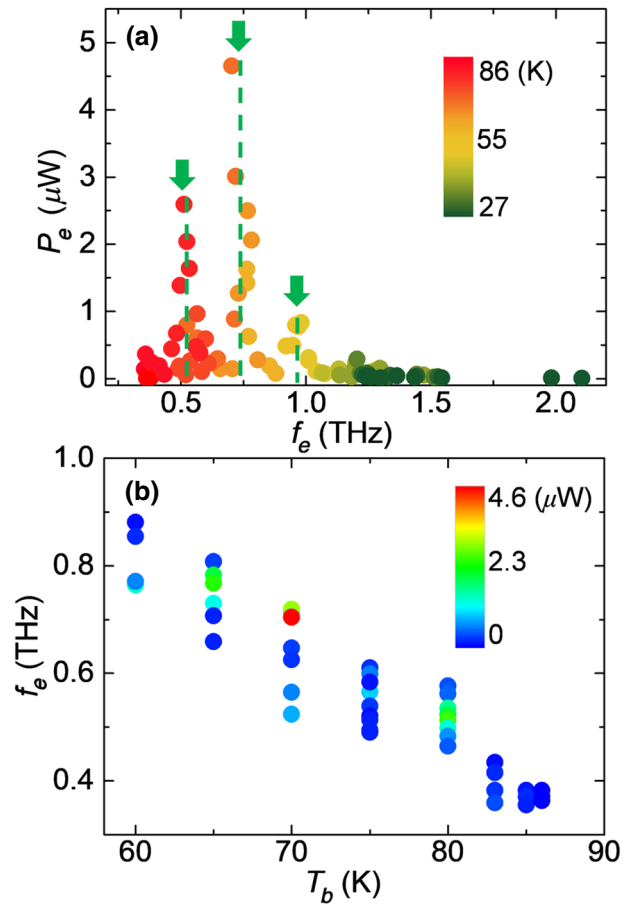
FIG. 4. (a) Emission power P_e vs emission frequency f_e [i.e., the peak positions and values taken from Fourier spectra such as the ones shown in Figs. 2(c) and 2(d)] at various T_b values indicated by the color code. Arrows and dashed lines indicate emission peaks. (b) Emission frequency f_e vs bath temperature for $T_b \geq 60$ K. The color code indicates the emission power P_e.

to its resistive state at $I \approx 96$ mA [see Fig. 3(a)]. Terahertz emission can be observed for currents up to 160 mA [see Fig. 3(b)], indicating that the temperature of the stack is below T_c at least up to this current. The maximum emission power of 2.68 μW is observed at $I = 117.2$ mA and a voltage of 0.603 V [bias point *C* in Fig. 3(a)]. Here, the emission frequency is 0.513 THz [see Fig. 3(d)]. Overall, the device emits radiation in the frequency range from 0.483 to 0.577 THz. The latter value, to our knowledge, is a record for operation above 77 K.

Figure 4(a) shows the emission power P_e vs emission frequency f_e at various color-coded T_b values. In Fig. 4(b) f_e is plotted vs T_b in the temperature range from 60 to 86 K, using P_e as color code. In this temperature range, the emitter has a frequency range tunable from 0.356 to 0.881 THz, which is much higher than that in earlier reports [25–27,29,35]. For bath temperatures between 27.8 and 86 K, as plotted in Fig. 4(a), emission is observed over a frequency range from 0.37 to 2.09 THz, with two prominent

peaks in P_e near 0.5 and 0.75 THz, and a smaller one near 0.95 THz. These peaks originate from measurements in the temperature ranges of 70–80 K, 60–70 K, and 50–55 K, respectively. These peaks are associated with cavity resonances. For a square IJJ stack, resonant modes were classified by Klemm *et al.* [63,64], and it was shown that, apart from resonances oscillating with k half waves along the length of the stack and l half waves along its width, because of degeneracy of resonant modes of the square geometry, there can be a number of mixed modes. Indeed, the emission peaks observed near 0.5 THz in Fig. 4(b) could match the TM$(1,1)$ mode predicted in Ref. [63] (0.51 THz), and the peak near 0.75 THz could match the degenerate TM$(0,2)$ and TM$(2,0)$ cavity resonance modes (0.71 THz).

To obtain more insight into the electrothermal behavior of the stack, particularly in view of high-temperature operation and in view of resonant modes, we simulate a 200×200 μm^2 stand-alone 600-junction stack with a critical

current density $j_c = 2$ kA/cm^2 using three-dimensional coupled sine-Gordon equations as in Ref. [61]. Some results are shown in Fig. 5 and some technical details are given in the Appendix. The model parameters used are a first guess and no actual fit to the experimental data is attempted. Figure 5(a) shows by points connected by lines IVCs at four different bath temperatures. The data points at $I = 120$ and 100 mA forming horizontal lines are obtained by sweeping the bath temperature between 70 and 55 K at fixed current. The shape of the IVCs is reasonably close to that of the experimental IVCs at the corresponding values of T_b, and we briefly mention here that similar simulations using a critical current density of 1 kA/cm^2 yielded much worse agreement with the experimental data, indicating that our estimate of j_c is not unreasonable. With respect to the IVCs in Fig. 5(a), at $T_b = 28$ K there is a hot spot in the stack for bias currents between 120 and 24 mA, which is located near one of the edges of the stack. At $I = 120$ mA the maximum (minimum) temperature in the stack is 150 K (30.5 K). With decreasing current the hot spot shrinks and dissolves below $I = 24$ mA, leading to a jump in the voltage across the stack toward large values. Near the hot-spot nucleation point the hot spot can be either present or absent in the stack depending on the initial temperature distribution. We make use of this fact at $I = 24$ mA where we use different initial temperature distributions $T > T_c$ and $T = T_b$ to obtain states with and without a hot spot. In the latter case the temperature in the stack varies only weakly, between 23.8 and 35.9 K, while in the former case the temperature varies between 30.5 and 100 K. For bath temperatures of 60, 70, and 80 K there is no hot spot. For example, at $T_b = 60$ K and $I = 120$ mA the temperature varies smoothly between 67 and 82.5 K, the maximum temperature being reached in the center of the stack. For lower currents the temperature variation decreases further. For $T_b = 70$ K we find a temperature variation between 77.8 and 82 K at $I = 120$ mA, and at $T_b = 70$ K we obtain a variation between 86.7 and 89 K at $I = 120$ mA.

The color scale in Fig. 5(a) is a measure for the emitted terahertz power, which we calculate via the Poynting vector integrated along the circumference of the stack. The highest values are obtained near $T_b = 60$ K and $I = 120$ mA. The emission power smoothly decreases when either the current is varied at $T_b = 60$ K or when the bath temperature is increased at fixed current. For lower bath temperatures the emitted power decreases more rapidly. Overall, the observed variation of the emitted power is much less than in the experiment.

At $T_b = 70$ K and $I = 100$ mA the simulated stack radiates at a frequency of 0.51 THz, which is close to one of the experimentally observed emission peaks in Fig. 4(a). For this bias point, Fig. 5(b) shows a map of the power density $\langle q_\parallel(x,y) \rangle$ dissipated by in-plane currents in the stack, averaged over time and the z direction and given in the unit
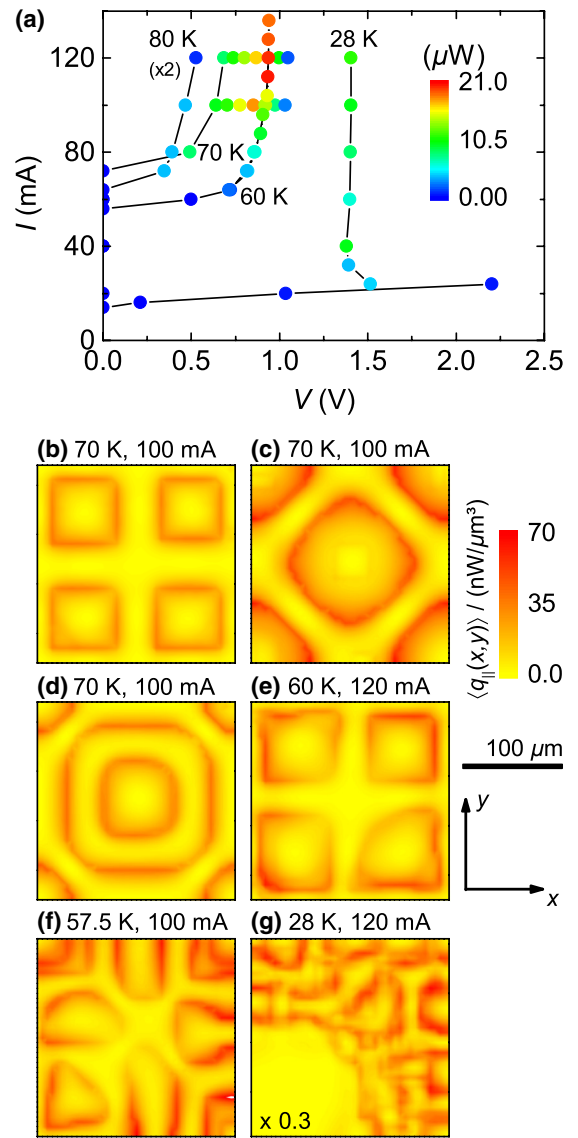

FIG. 5. Results of numerical simulation for a 200×200 μm^2 stand-alone 600-junction stack with a critical current density $j_c = 2$ kA/cm^2. (a) Outermost branch of the IVCs for four different bath temperatures (points connected by lines). Additional points at $I = 120$ and 100 mA are obtained by our sweeping the bath temperature at fixed current. The color scale indicates the emission power, calculated from the Poynting vector taken along the circumference of the stack. (b)–(g) Color maps showing the in-plane distribution of the power density $\langle q_\parallel(x,y) \rangle$ dissipated by in-plane currents, averaged over time and the z direction. (b),(c),(d): $T_b = 70$ K, $I = 100$ mA; (e) $T_b = 60$ K, $I = 120$ mA; (f) $T_b = 57.5$ K, $I = 100$ mA; (g) $T_b = 28$ K, $I = 120$ mA. In (g) the power scale is multiplied by 0.3.

of nanowatts per cubic micrometer. The pattern consisting of four ring structures where $\langle q_\parallel(x,y) \rangle$ is large, builds up spontaneously from an initially homogeneous phase distribution after some 10^3 Josephson-oscillation periods and is stable for at least 10^4 oscillation periods (about 20 ns).

Regions of high dissipation in this type of plot coincide with regions where columns (in the z direction) of fluxons and antifluxons have formed in the stack [60,61]. This means that for the pattern in Fig. 5(b) these fluxons and antifluxons form closed loops. Fig. 5(c) and 5(d) show maps for the *same* bias point $I = 100$ mA and $T_b = 70$ K. For these plots we *trigger* various patterns by choosing initial conditions for the Josephson phase difference, consisting of one or two straight columns of alternating fluxons and antifluxons extending along the x direction and the y direction. The ringlike shape forms after some waiting time and is again stable over at least 10^4 oscillation periods. In addition, we are able to stabilize patterns where four or five columns extend along x or y (i.e., $(0, k)$ or $(l, 0)$ modes), and we also stabilize, for example, $(5,5)$ modes this way. The fact that so many patterns are able to exist at the same bias indicates that the quality factor of these resonant modes is poor (presumably well below 10); that is, we should not expect distinct "resonant" peaks in a plot of emission power vs frequency. Figure 5(e) shows $\langle q_\parallel(x,y)\rangle$ for the point of maximum emission at $I = 120$ mA and $T_b = 60$ K. The pattern is similar to the one in Fig. 5(b); however, the fluxon rings look somewhat less regular. We observe patterns similar to the ones in Figs. 5(b) and 5(e) over the whole range of the 80- and 70-K IVCs, and for the 60-K IVC for bias currents down to 80 mA. In this range the emission frequency varies by more than a factor of 2, consistent with the assumption of a poor quality factor of the resonant modes. For bath temperatures below 60 K the $\langle q_\parallel(x,y)\rangle$ patterns become much more irregular. Figure 5(f) shows this for $T_b = 57.5$ K and $I = 100$ mA, where the center part of the stack is at a temperature close to T_c. Figure 5(g) shows an example for $T_b = 28$ K and $I = 120$ mA, where a hot spot has formed in the lower left part of the stack. For the present stack our simulations never yield regular patterns in the hot-spot region, indicating that for the high-current-density stack stable phase-lock of the IJJs in the stack is achieved only at high bath temperatures in the absence of a hot spot. The simulations do not consider effects such as statistical variations and c-axis gradients of, for example, the resistivity or the supercurrent density. These effects are likely to be present in the experimental stack and may further reduce the ability of the IJJs to phase-lock, such that a strong emission power appears only at some fortunate biasing conditions.

Finally, for the bias points below 25 mA in the $T_b = 28$ K IVC in Fig. 5(a) no fluxon/antifluxon pattern is excited in the stack. There is still emission but with power below 0.5 μW.

The simulated patterns in Figs. 5(b)–5(f) are in very good agreement with the patterns shown in Figs. 1 and 2 in Ref. [63]. Also in agreement with the predictions in Refs. [63,64] we do not see TM(n, m) modes with n and m not differing by a multiple of 2. Thus our work most likely confirms the predictions in those papers.

IV. CONCLUSIONS

In summary, using a slightly overdoped BSCCO crystal with high T_c and j_c we fabricate a stand-alone IJJ stack with good double-sided cooling. Using a Stirling cryocooler, we study the transport and emission properties at bath temperatures ranging from 27.8 to 86 K. By varying T_b and the bias current, we achieve continuous terahertz emission with emission frequencies from 0.356 to 2.09 THz. We also observe that the device can emit powerful terahertz waves in the liquid-nitrogen temperature range, with a record measured high emission frequency of 0.577 THz at $T_b = 80$ K, which is very interesting for potential applications using liquid nitrogen as a coolant. In plots of emission power P_e vs emission frequency f_e we observed resonancelike distinct peaks, arising from data obtained at bath temperatures between 60 and 80 K. In this temperature range, numerical simulations reveal regular patterns of the power density dissipated by in-plane currents, consisting of ring-shaped structures. A maximum in P_e vs f_e is observed, which, however, is much less pronounced than in the experiment. We argue that the peak structures seen in simulations and in the experiment are more related to the ability of the IJJs in the stack to phase-lock than to the resonance curve of a cavity mode.

APPENDIX: TECHNICAL DETAILS OF NUMERICAL SIMULATIONS

The basic model is described in Refs. [60,61]. Here we give a short summary, with a focus on changes relative to the model discussed in Ref. [61]. The electrical and thermal model parameters depend on temperature, and thus, for an inhomogeneous temperature distribution, on x, y, and z. Their spatial variation, as well as $T(x, y, z)$, are found by our self-consistently solving the thermal equations (requiring Joule heat dissipation as an input from the electric circuit) and the electrical equations (requiring the temperature distribution in the stack, as determined from the thermal circuit). In the present paper we consider

a stand-alone IJJ stack (rather than a mesa) consisting of $N = 600$ IJJs. The stack has a length $L_s = 200$ μm along x and a width $W_s = 200$ μm along y. It is covered by two gold layers and clamped between two substrates, their outer surfaces kept at T_b. In the experiment, between the lower substrate and the lower electrode of the BSCCO stack there is a glue layer with thickness that is not well defined, and there are various Kapitza resistances between the different layers (e.g., between the upper Au electrode and the upper substrates or between the Au electrodes and the BSCCO stack). To keep the calculations simple we assume that between each substrate and the BSCCO stack there is a layer with poor thermal conductivity κ_g and thickness d_g that we use as a fit parameter to roughly match the IVC at $I = 120$ mA and T_b to the experimental curve. For the simulations presented we take $d_g = 10$ μm and $\kappa_g = 1$ W/(m K). We further assume for the thermal description that the IJJ stack plus the contacting Au layer has a temperature $T_m(x,y)$ that is constant along z but can vary along x and y. For the BSCCO thermal conductivity we use the same values and temperature dependencies as in Ref. [60]. In the z direction the substrates [thickness 100 μm, thermal conductivity 1000 W/(m K)] are discretized by two segments, and each poorly conducting sheet is discretized by nine segments. For this geometry we solve the heat-diffusion equation $c\,dT/dt = \nabla(\kappa\nabla T) + q_s$, with specific heat capacity c, (anisotropic and layer-dependent) thermal conductivity κ, and power density q_s for heat generation in the stack.

For the electric circuit we group the N IJJs in the stack to M segments, each containing $G = N/M$ IJJs, assumed to have identical properties. During many calculations, it turns out that the solutions (electric field and current distributions) we obtain are independent of G, provided that they are stable in general, are captured by the discretization used along the x and y directions, and G is low enough. It turns out that the minimum value of G to reach stability increases with increasing j_c; for the present studies it is below 10.

In the model the electric current density j_{ext} is injected into the Au layer, which we assume to have a low enough resistance to freely distribute the current before it enters the IJJ stack in the z direction with a density $j_{z,\text{Au}}$ proportional to the local BSCCO conductance $\sigma_c(x,y) = \rho_c^{-1}(x,y)$. The full expression is $j_{z,\text{Au}} = \langle j_{\text{ext}}\rangle \sigma_c(x,y)/\langle\sigma_c\rangle$, the brackets denoting spatial averaging. The same current leaves the lower Au electrode. The z-axis currents consist of Josephson currents with critical current density $j_c(x,y)$, (ohmic) quasiparticle currents with resistivity $\rho_c(x,y)$, and displacement currents with (temperature-independent) dielectric constant ε. For the temperature dependence of j_c we use a parabolic profile, $j_c \propto 1 - (T/T_c)^2$; for the temperature dependence of ρ_c, see Ref. [60]. To avoid weakly stable solutions we also add Nyquist noise created by the quasiparticle currents. The in-plane currents consist

of a superconducting part, characterized by a Cooper-pair density $n_s(x,y)$, a quasiparticle component with resistivity $\rho_{ab}(x,y)$, and a Nyquist-noise component. For constant $T_m(x,y) = 4.2$ K we index the above quantities by an additional "0" and assume that they are constant with respect to x and y. The temperature dependence of the various parameters is close to the experimental curves and is plotted in detail in Ref. [60]. We further use $T_c = 91.5$ K.

We obtain sine-Gordon-like equations for the Josephson phase differences $\gamma_m(x,y)$ in the mth segment of the IJJ stack [76]:

$$Gsd_s\nabla\left(\frac{\nabla\dot{\gamma}_m}{\rho_{ab}}\right) + d_s\nabla(j_{x,m+1}^N - j_{x,m}^N) + G\lambda_k^2\nabla(n_s\nabla\gamma_m)$$
$$= \left(2 + \frac{G^2\lambda_k^2 n_s}{\lambda_c^2}\right)j_{z,m} - j_{z,m+1} - j_{z,m-1}. \quad (A1)$$

Here $m = 1,\dots,M$, $\nabla = (\partial/\partial x, \partial/\partial y)$, $d_s = 0.5$ nm is the thickness of the superconducting layers, and $\lambda_k = [\Phi_0 d_s/(2\pi\mu_0 j_{c0}\lambda_{ab0}^2)]^{1/2}$, with the in-plane London penetration depth λ_{ab0} and the magnetic permeability μ_0. $\lambda_c = [\Phi_0/(2\pi\mu_0 j_{c0}s)]^{1/2}$ is the out-of-plane penetration depth. Quantities $j_{x,m}^N$ are the in-plane noise current densities. Time is normalized to $\Phi_0/2\pi j_{c0}\rho_{c0}s$, resistivities are normalized to ρ_{c0}, and current densities are normalized to j_{c0}.

For the out-of-plane current densities $j_{z,m}$ one finds [77]

$$j_{z,m} = \frac{\beta_{c0}}{G}\ddot{\gamma}_m + \frac{\dot{\gamma}_m}{\rho_{c,m}} + j_c\sin\gamma_m + j_{z,m}^N, \quad (A2)$$

where $\beta_{c0} = 2\pi j_{c0}\rho_{c0}^2\varepsilon\varepsilon_0 s/\Phi_0$, $s = 1.5$ nm is the interlayer period, ε_0 is the vacuum permittivity, and the $j_{z,m}^N$ are the out-of-plane noise current densities. The in-plane densities are calculated as in Ref. [61]. For the electrical parameters we used the 4.2-K values $\rho_{c0} = 800$ Ω cm, $j_{c0} = 2$ kA/cm^2, and $\lambda_{ab0} = 260$ nm, and further $\rho_{ab}(T_c) = 8$ $\mu\Omega$ cm and $\varepsilon = 9$, yielding $\lambda_c = 93.5$ μm, $\lambda_k = 0.31$ μm, and $\beta_{c0} = 4.64 \times 10^5$.

To calculate IVCs the differential equations are discretized with use of 20 grid points along x and y. This low resolution is necessary to keep the computation time reasonable. To calculate the $\langle q_\parallel(x,y)\rangle$ patterns shown in Fig. 5 we use 40 grid points in each direction. We further use $M = 100$ for calculations at bath temperatures above 50 K and $M = 150$ for $T_b = 28$ K. A fifth-order Runge-Kutta scheme is used to evolve the above equations in time.

For a given set of input parameters, in a first initializing step we solve the heat-diffusion equation considering dissipation by out-of-plane quasiparticle currents only, to achieve stationary distributions for the temperature and j_{ext}. Far away from the hot-spot nucleation point the initial temperature does not matter very much, and we use a value above T_c. Near the hot-spot nucleation point there is hysteresis; that is, temperature distribution with or without

a hot spot can be realized, depending on the initial temperature in the stack. Then, in a second initializing step, heat-diffusion and sine-Gordon equations are solved simultaneously over typically 5000 Josephson oscillations. In most simulations we start with a constant phase γ and just evolve the dynamics over time. In some cases we trigger solutions, by using cosine profiles of γ, alternating between adjacent layers. This triggers fluxon-antifluxon rows. After the initialization steps [60] various quantities, partially averaged over spatial coordinates, are tracked as a function of time to produce time averages or to make Fourier transforms.

[1] M. Tonouchi, Cutting-edge terahertz technology, Nat. Photonics **1**, 97 (2007).

[2] B. Ferguson, and X. C. Zhang, Materials for terahertz science and technology, Nat. Mater. **1**, 26 (2002).

[3] U. Welp, K. Kadowaki, and R. Kleiner, Superconducting emitters of THz radiation, Nat. Photonics **7**, 702 (2013).

[4] I. Kakeya, and H. B. Wang, Terahertz-wave emission from Bi2212 intrinsic Josephson junctions: A review on recent progress, Supercond. Sci. Technol. **29**, 073001 (2016).

[5] T. Kashiwagi, H. Kubo, K. Sakamoto, T. Yuasa, Y. Tanabe, C. Watanabe, T. Tanaka, Y. Komori, R. Ota, G. Kuwano, K. Nakamura, T. Katsuragawa, M. Tsujimoto, T. Yamamoto, R. Yoshizaki, H. Minami, K. Kadowaki, and R. A. Klemm, The present status of high-T_c superconducting terahertz emitters, Supercond. Sci. Technol. **30**, 074008 (2017).

[6] L. Ozyuzer, A. E. Koshelev, C. Kurter, N. Gopalsami, Q. Li, M. Tachiki, K. Kadowaki, T. Yamamoto, H. Minami, H. Yamaguchi, T. Tachiki, K. E. Gray, W.-K. Kwok, and U. Welp, Emission of coherent THz radiation from superconductors, Science **318**, 1291 (2007).

[7] K. Kadowaki, H. Yamaguchi, K. Kawamata, T. Yamamoto, H. Minami, I. Kakeya, U. Welp, L. Ozyuzer, A. Koshelev, C. Kurter, K. E. Gray, and W.-K. Kwok, Direct observation of tetrahertz electromagnetic waves emitted from intrinsic Josephson junctions in single crystalline Bi2Sr2CaCu2O8+δ, Physica C **468**, 634 (2008).

[8] H. B. Wang, S. Guénon, J. Yuan, A. Iishi, S. Arisawa, T. Hatano, T. Yamashita, D. Koelle, and R. Kleiner, Hot Spots and Waves in Bi2Sr2CaCu2O8 Intrinsic Josephson Junction Stacks: A Study by Low Temperature Scanning Laser Microscopy, Phys. Rev. Lett. **102**, 017006 (2009).

[9] H. Minami, I. Kakeya, H. Yamaguchi, T. Yamamoto, and K. Kadowaki, Characteristics of terahertz radiaton emitted from the intrinsic Josephson junctions in high-T_c superconductor Bi2Sr2CaCu2O8+δ, Appl. Phys. Lett. **95**, 232511 (2009).

[10] K. E. Gray, L. Ozyuzer, A. E. Koshelev, C. Kurter, K. Kadowaki, T. Yamamoto, H. Minami, H. Yamaguchi, M. Tachiki, W.-K. Kwok, and U. Welp, Emission of terahertz waves from stacks of intrinsic Josephson junctions, IEEE Trans. Appl. Supercond. **19**, 3755 (2009).

[11] S. Guénon, M. Grünzweig, B. Gross, J. Yuan, Z. G. Jiang, Y. Y. Zhong, A. Iishi, P. H. Wu, T. Hatano, D. Koelle, H. B. Wang, and R. Kleiner, Interaction of hot spots and THz waves in Bi2Sr2CaCu2O8 intrinsic Josephson junction stacks of various geometry, Phys. Rev. B **82**, 214506 (2010).

[12] C. Kurter, L. Ozyuzer, T. Proslier, J. F. Zasadzinski, D. G. Hinks, and K. E. Gray, Counterintuitive consequence of heating in strongly-driven intrinsic junctions of Bi2Sr2CaCu2O8+δ mesas, Phys. Rev. B **81**, 224518 (2010).

[13] H. B. Wang, S. Guénon, B. Gross, J. Yuan, Z. G. Jiang, Y. Y. Zhong, M. Gruenzweig, A. Iishi, P. H. Wu, T. Hatano, D. Koelle, and R. Kleiner, Coherent Terahertz Emission of Intrinsic Josephson Junction Stacks in the Hot Spot Regime, Phys. Rev. Lett. **105**, 057002 (2010).

[14] M. Tsujimoto, K. Yamaki, K. Deguchi, T. Yamamoto, T. Kashiwagi, H. Minami, M. Tachiki, K. Kadowaki, and R. A. Klemm, Geometrical Resonance Conditions for THz Radiation from the Intrinsic Josephson Junctions in Bi2Sr2CaCu2O8+δ, Phys. Rev. Lett. **105**, 037005 (2010).

[15] H. Koseoglu, F. Turkoglu, Y. Simsek, and L. Ozyuzer, The fabrication of THz emitting mesas by reactive ion-beam etching of superconducting Bi2212 with multilayer masks, J. Supercond. Nov. Magn. **24**, 1083 (2011).

[16] T. M. Benseman, A. E. Koshelev, K. E. Gray, W.-K. Kwok, U. Welp, K. Kadowaki, M. Tachiki, and T. Yamamoto, Tunable terahertz emission from Bi2Sr2CaCu2O8+δ mesa devices, Phys. Rev. B **84**, 064523 (2011).

[17] J. Yuan, M. Y. Li, J. Li, B. Gross, A. Ishii, K. Yamaura, T. Hatano, K. Hirata, E. Takayama-Muromachi, P. H. Wu, D. Koelle, R. Kleiner, and H. B. Wang, Terahertz emission from Bi2Sr2CaCu2O8+δ intrinsic Josephson junction stacks with all-superconducting electrodes, Supercond. Sci. Technol. **25**, 075015 (2012).

[18] M. Y. Li, J. Yuan, N. Kinev, J. Li, B. Gross, S. Guénon, A. Ishii, K. Hirata, T. Hatano, D. Koelle, R. Kleiner, V. P. Koshelets, H. B. Wang, and P. H. Wu, Linewidth dependence of coherent terahertz emission from Bi2Sr2CaCu2O8 intrinsic Josephson junction stacks in the hot-spot regime, Phys. Rev. B **86**, 060505(R) (2012).

[19] I. Kakeya, Y. Omukai, T. Yamamoto, K. Kadowaki, and M. Suzuki, Effect of thermal inhomogeneity for terahertz radiation from intrinsic Josephson junction stacks of Bi2Sr2CaCu2O8+δ, Appl. Phys. Lett. **100**, 242603 (2012).

[20] T. Kashiwagi, M. Tsujimoto, T. Yamamoto, H. Minami, K. Yamaki, K. Delfanazari, K. Deguchi, N. Orita, T. Koike, R. Nakayama, T. Kitamura, M. Sawamura, S. Hagino, K. Ishida, K. Ivanovic, H. Asai, M. Tachiki, R. A. Klemm, and K. Kadowaki, High temperature superconductor terahertz emitters: Fundamental physics and its applications, J. J. Appl. Phys. **51**, 010113 (2012).

[21] T. M. Benseman, A. E. Koshelev, W.-K. Kwok, U. Welp, V. K. Vlasko-Vlasov, K. Kadowaki, H. Minami, and C. Watanabe, Direct imaging of hot spots in Bi2Sr2CaCu2O8+δ mesa terahertz sources, J. Appl. Phys. **113**, 133902 (2013a).

[22] T. M. Benseman, K. E. Gray, A. E. Koshelev, W.-K. Kwok, U. Welp, H. Minami, K. Kadowaki, and T. Yamamoto, Powerful terahertz emission from Bi2Sr2CaCu2O8+δ mesa arrays, Appl. Phys. Lett. **103**, 022602 (2013b).

[23] S. Sekimoto, C. Watanabe, H. Minami, T. Yamamoto, T. Kashiwagi, R. A. Klemm, and K. Kadowaki, Continuous 30 μW terahertz source by a high-T_c superconductor mesa structure, Appl. Phys. Lett. **103**, 182601 (2013).

[24] H. Minami, C. Watanabe, K. Sato, S. Sekimoto, T. Yamamoto, T. Kashiwagi, R. A. Klemm, and K. Kadowaki, Local SiC photoluminescence evidence of hot spot formation and sub-THz coherent emission from a rectangular $Bi_2Sr_2CaCu_2O_{8+x}$ mesa, Phys. Rev. B **89**, 054503 (2014).

[25] M. Ji, J. Yuan, B. Gross, F. Rudau, D. Y. An, M. Y. Li, X. J. Zhou, Y. Huang, H. C. Sun, Q. Zhu, J. Li, N. Kinev, T. Hatano, V. P. Koshelets, D. Koelle, R. Kleiner, W. W. Xu, B. B. Jin, H. B. Wang, and P. H. Wu, $Bi_2Sr_2CaCu_2O_8$ intrinsic Josephson junction stacks with improved cooling: Coherent emission above 1 THz, Appl. Phys.Lett. **105**, 122602 (2014).

[26] T. Kashiwagi, T. Yamamoto, T. Kitamura, K. Asanuma, C. Watanabe, K. Nakade, T. Yasui, Y. Saiwai, Y. Shibano, H. Kubo, K. Sakamoto, T. Katsuragawa, M. Tsujimoto, K. Delfanazari, R. Yoshizaki, H. Minami, R. A. Klemm, and K. Kadowaki, Generation of electromagnetic waves from 0.3 to 1.6 terahertz with a high-T_c superconducting $Bi_2Sr_2CaCu_2O_{8+\delta}$ intrinsic Josephson junctionemitter, Appl. Phys. Lett. **106**, 092601 (2015a).

[27] T. Kashiwagi, K. Sakamoto, H. Kubo, Y. Shibano, T. Enomoto, T. Kitamura, K. Asanuma, T. Yasui, C. Watanabe, K. Nakade, Y. Saiwai, T. Katsuragawa, M. Tsujimoto, R. Yoshizaki, T. Yamamoto, H. Minami, R. A. Klemm, and K. Kadowaki, A high-T_c intrinsic Josephson junction emitter tunable from 0.5 to 2.4 terahertz, Appl. Phys. Lett. **107**, 082601 (2015b).

[28] X. J. Zhou, Q. Zhu, M. Ji, D. Y. An, L. Y. Hao, H. C. Sun, S. Ishida, F. Rudau, R. Wieland, J. Li, D. Koelle, H. Eisaki, Y. Yoshida, T. Hatano, R. Kleiner, H. B. Wang, and P. H. Wu, Three-terminal stand-alone superconducting terahertz emitter, Appl. Phys. Lett. **107**, 122602 (2015).

[29] L. Y. Hao, M. Ji, J. Yuan, D. Y. An, M. Y. Li, X. J. Zhou, Y. Huang, H. C. Sun, Q. Zhu, F. Rudau, R. Wieland, N. Kinev, J. Li, W. W. Xu, B. B. Jin, J. Chen, T. Hatano, V. P. Koshelets, D. Koelle, R. Kleiner, H. B. Wang, and P. H. Wu, Compact Superconducting Terahertz Source Operating in Liquid Nitrogen, Phys. Rev. Appl. **3**, 024006 (2015).

[30] T. Kashiwagi, T. Yamamoto, H. Minami, M. Tsujimoto, R. Yoshizaki, K. Delfanazari, T. Kitamura, C. Watanabe, K. Nakade, T. Yasui, K. Asanuma, Y. Saiwai, Y. Shibano, T. Enomoto, H. Kubo, K. Sakamoto, T. Katsuragawa, B. Marković, J. Mirković, R. A. Klemm, and K. Kadowaki, Efficient Fabrication of Intrinsic-Josephson-Junction Terahertz Oscillators with Greatly Reduced Self-heating Effects, Phys. Rev. Applied **4**, 054018 (2015).

[31] C. Watanabe, H. Minami, T. Kitamura, K. Asanuma, K. Nakade, T. Yasui, Y. Saiwai, Y. Shibano, T. Yamamoto, T. Kashiwagi, R. A. Klemm, and K. Kadowaki, Influence of the local heating position on the terahertz emission power from high-T_c superconducting $Bi_2Sr_2CaCu_2O_{8+\delta}$ mesas, Appl. Phys. Lett. **106**, 042603 (2015).

[32] M. Tsujimoto, Y. Maeda, H. Kambara, A. Elarabi, Y. Yoshioka, Y. Nakagawa, Y. Wen, T. Doi, H. Saito, and I. Kakeya, Terahertz emission from a stack of intrinsic Josephson junctions in Pb-doped $Bi_2Sr_2CaCu_2O_{8+\delta}$, Supercond. Sci. Technol. **28**, 105015 (2015).

[33] M. Tsujimoto, I. Kakeya, T. Kashiwagi, H. Minami, and K. Kadowaki, Cavity mode identification for coherent terahertz emission from high-T_c superconductors, Opt. Express **24**, 4591 (2016).

[34] M. Tsujimoto, T. Doi, G. Kuwano, A. Elarabi, and I. Kakeya, Engineering and characterization of a packaged high-T_c superconducting terahertz source module, Supercond. Sci. Technol. **30**, 064001 (2017).

[35] Y. Huang, H. C. Sun, D. Y. An, X. J. Zhou, M. Ji, F. Rudau, R. Wieland, J. S. Hampp, O. Kizilaslan, J. Yuan, N. Kinev, O. Kiselev, V. P. Koshelets, J. Li, D. Koelle, R. Kleiner, B. B. Jin, J. Chen, L. Kang, W. W. Xu, H. B. Wang, and P. H. Wu, Self-mixing Spectra of Terahertz Emitters based on $Bi_2Sr_2CaCu_2O_{8+\delta}$ Intrinsic Josephson-junction Stacks, Phys. Rev. Applied **8**, 054023 (2017).

[36] A. Elarabi, Y. Yoshioka, M. Tsujimoto, and I. Kakeya, Monolithic Superconducting Emitter of Tunable Circularly Polarized Terahertz Radiation, Phys. Rev. Applied **8**, 064034 (2017).

[37] E. A. Borodianskyi and V. M. Krasnov, Josephson emission with frequency span 1-11 THz from small $Bi_2Sr_2CaCu_2O_{8+\delta}$ mesa structures, Nat. Commun. **8**, 1742 (2017).

[38] T. Kashiwagi, T. Tanaka, C. Watanabe, H. Kubo, Y. Komori, T. Yuasa, Y. Tanabe, R. Ota, G. Kuwano, K. Nakamura, M. Tsujimoto, H. Minami, T. Yamamoto, R. A. Klemm, and K. Kadowaki, Thermoreflectance microscopy measurements of the Joule heating characteristics of high-T_c superconducting terahertz emitters, J. Appl. Phys. **122**, 233902 (2017).

[39] L. N. Bulaevskii and A. E. Koshelev, Radiation Due to Josephson Oscillations in Layered Superconductors, Phys. Rev. Lett. **99**, 057002 (2007).

[40] A. E. Koshelev, Alternating dynamic state self-generated by internal resonance in stacks of intrinsic Josephson junctions, Phys. Rev. B **79**, 174509 (2008).

[41] Shizeng Lin and Xiao Hu, Possible Dynamic States in Inductively Coupled Intrinsic Josephson Junctions of Layered High-T_c Superconductors, Phys. Rev. Lett. **100**, 247006 (2008).

[42] V. M. Krasnov, Nonlinear Nonequilibrium Quasiparticle Relaxation in Josephson Junctions, Phys. Rev. Lett. **103**, 227002 (2009).

[43] R. A. Klemm and K. Kadowaki, Output from a Josephson stimulated terahertz amplified radiation emitter, J. Phys. Cond. Mat. **22**, 375701 (2010).

[44] N. F. Pedersen and S. Madsen, THz generation using fluxon dynamics in high temperature superconductors, IEEE Trans. Appl. Supercond. **19**, 726 (2009).

[45] X. Hu and S. Z. Lin, Cavity phenomena in mesas of cuprate high-T_c superconductors under voltage bias, Phys. Rev. B **80**, 064516 (2009).

[46] T. Koyama, H. Matsumoto, M. Machida, and K. Kadowaki, In-phase electrodynamics and terahertz wave emission in extended intrinsic Josephson junctions, Phys. Rev. B **79**, 104522 (2009).

[47] K. Kadowaki, M. Tsujimoto, K. Yamaki, T. Yamamoto, T. Kashiwagi, H. Minami, M. Tachiki, and R. A. Klemm, Evidence for a dual-source mechanism of THz radiation from rectangular mesas of single crystalline $Bi_2Sr_2CaCu_2 O_{8+\delta}$ intrinsic Josephson junctions, J. Phys. Soc. Jpn. **79**, 023703 (2010).

[48] V. M. Krasnov, Coherent flux-flow emission from stacked Josephson junctions: Nonlocal radiative boundary

conditions and the role of geometrical resonances, Phys. Rev. B **82**, 134524 (2010).

[49] A. E. Koshelev, Stability of dynamic coherent states in intrinsic Josephson-junction stacks near internal cavity resonance, Phys. Rev. B **82**, 174512 (2010).

[50] A. Yurgens, Temperature distribution in a large $Bi_2Ca Cu_2O_{8+\delta}$ mesa, Phys. Rev. B **83**, 184501 (2011).

[51] V. M. Krasnov, Terahertz electromagnetic radiation from intrinsic Josephson junctions at zero magnetic field via breather-type self-oscillations, Phys. Rev. B **83**, 174517 (2011).

[52] M. Tachiki, K. Ivanovic, K. Kadowaki, and T. Koyama, Emission of terahertz electromagnetic waves from intrinsic Josephson junction arrays embedded in resonance LCR circuits, Phys.Rev. B **83**, 014508 (2011).

[53] H. Asai, M. Tachiki, and K. Kadowaki, Three-dimensional numerical analysis of terahertz radiation emitted from intrinsic Josephson junctions with hot spots, Phys. Rev. B **85**, 064521 (2011).

[54] S. Z. Lin and X. Hu, In-plane dissipation as a possible synchronization mechanism for terahertz radiation from intrinsic Josephson junctions of layered superconductors, Phys. Rev. B **86**, 054506 (2012).

[55] Yu. O. Averkov, V. M. Yakovenko, V. A. Yampolskii, and F. Nori, Conversion of Terahertz Wave Polarization at the Boundary of a Layered Superconductor Due to the Resonance Excitation of Oblique Surface Waves, Phys. Rev. Lett. **109**, 027005 (2012).

[56] A. Grib and P. Seidel, The influence of standing waves on synchronization and self-heating of Josephson junctions in resonant systems, Low Temp. Phys. **38**, 321 (2012).

[57] B. Gross, S. Guénon, J. Yuan, M. Y. Li, J. Li, A. Ishii, R. G. Mints, T. Hatano, P. H. Wu, D. Koelle, H. B. Wang, and R. Kleiner, Hot-spot formation in stacks of intrinsic Josephson junctions in $Bi_2Sr_2CaCu_2O_8$, Phys. Rev. B **86**, 094524 (2012).

[58] B. Gross, J. Yuan, D. Y. An, M. Y. Li, N. Kinev, X. J. Zhou, M. Ji, Y. Huang, T. Hatano, R. G. Mints, V. P. Koshelets, P. H. Wu, H. B. Wang, D. Koelle, and R. Kleiner, Modeling the linewidth dependence of coherent terahertz emission from intrinsic Josephson junction stacks in the hot-spot regime, Phys. Rev. B **88**, 014524 (2013).

[59] H. Asai and S. Kawabata, Intense terahertz emission from intrinsic Josephson junctions by external heat control, Appl. Phys. Lett. **101**, 112601 (2014).

[60] F. Rudau, M. Tsujimoto, B. Gross, T. E. Judd, R. Wieland, E. Goldobin, N. Kinev, J. Yuan, Y. Huang, M. Ji, X. J. Zhou, D. Y. An, A. Ishii, R. G. Mints, P. H. Wu, T. Hatano, H. B. Wang, V. P. Koshelets, D. Koelle, and R. Kleiner, Thermal and electromagnetic properties of $Bi_2Sr_2CaCu_2O_8$ intrinsic Josephson junction stacks studied via one-dimensional coupled sine-Gordon equations, Phys. Rev. B **91**, 104513 (2015).

[61] F. Rudau, R. Wieland, J. Langer, X. J. Zhou, M. Ji, N. Kinev, L. Y. Hao, Y. Huang, J. Li, P. H. Wu, T. Hatano, V. P. Koshelets, H. B. Wang, D. Koelle, and R. Kleiner, 3D Simulations of the Electrothermal and THz Emission Properties of $Bi_2Sr_2CaCu_2O_8$ Intrinsic Josephson Junction Stacks, Phys. Rev. Appl. **5**, 044017 (2016).

[62] D. P. Cerkoney, C. Reid, C. M. Doty, A. Gramajo, T. D. Campbell, M. A. Morales, K. Delfanazari, M. Tsujimoto,

T. Kashiwagi, T. Yamamoto, C. Watanabe, H. Minami, K. Kadowaki, and R. A. Klemm, Cavity mode enhancement of terahertz emission from equilateral triangular microstrip antennas of the high-T_c superconductor $Bi_2Sr_2CaCu_2O_{8+\delta}$, J. Phys.: Condens. Matter **29**, 015601 (2017).

[63] R. A. Klemm, A. E. Davis, and Q. X. Wang, Terahertz emission from thermally managed square intrinsic Josephson junction microstrip antennas, IEEE J. Sel. Top. Quant. Electron. **23**, 8501208 (2017a).

[64] R. A. Klemm, A. E. Davis, Q. X. Wang, T. Yamamoto, D. P. Cerkoney, C. Reid, M. L. Koopman, H. Minami, T. Kashiwagi, J. R. Rain, C. M. Doty, M. A. Sedlack, M. A. Morales, C. Watanabe, M. Tsujimoto, K. Delfanazari, and K. Kadowaki, Terahertz emission from the intrinsic Josephson junctions of high-symmetry thermally-managed $Bi_2Sr_2CaCu_2O_{8+\delta}$ microstrip antennas, IOP Conf. Ser.: Mater. Sci.Eng. **279**, 012017 (2017b).

[65] M. Tsujimoto, H. Minami, K. Delfanazari, M. Sawamura, R. Nakayama, T. Kitamura, T. Yamamoto, T. Kashiwagi, T. Hattori, and K. Kadowaki, Terahertz imaging system using high-T_c superconducting oscillation devices, J. Appl. Phys. **111**, 123111 (2012).

[66] T. Kashiwagi, K. Nakade, Y. Saiwai, H. Minami, T. Kitamura, C. Watanabe, K. Ishida, S. Sekimoto, K. Asanuma, T. Yasui, Y. Shibano, M. Tsujimoto, T. Yamamoto, B. Markovic, J. Mirkovic, R. A. Klemm, and K. Kadowaki, Computed tomography image using sub-terahertz waves generated from a high-T_c superconducting intrinsic Josephson junction oscillator, Appl. Phys. Lett. **104**, 082603 (2014a).

[67] T. Kashiwagi, K. Nakade, B. Markovic, Y. Saiwai, H. Minami, T. Kitamura, C. Watanabe, K. Ishida, S. Sekimoto, K. Asanuma, T. Yasui, Y. Shibano, M. Tsujimoto, T. Yamamoto, J. Mirkovic, and K. Kadowaki, Reflection type of terahertz imaging system using a high-T_c superconducting oscillator, Appl. Phys. Lett. **104**, 022601 (2014b).

[68] K. Nakade, T. Kashiwagi, Y. Saiwai, H. Minami, T. Yamamoto, R. A. Klemm, and K. Kadowaki, Applications using high-T_c superconducting terahertz emitters, Sci. Rep. **6**, 23178 (2016).

[69] H. C. Sun, Z. B. Yang, N. V. Kinev, O. S. Kiselev, Y. Y. Lv, Y. Huang, L. Y. Hao, X. J. Zhou, M. Ji, X. C. Tu, C. H. Zhang, J. Li, F. Rudau, R. Wieland, J. S. Hampp, O. Kizilaslan, D. Koelle, B. B. Jin, J. Chen, L. Kang, W. W. Xu, R. Kleiner, V. P. Koshelets, H. B. Wang, and P. H. Wu, Terahertz Spectroscopy of Dilute Gases using $Bi_2Sr_2CaCu_2O_{8+\delta}$ Intrinsic Josephson-junction Stacks, Phys. Rev. Applied **8**, 054005 (2017).

[70] D. Y. An, J. Yuan, N. Kinev, M. Y. Li, Y. Huang, M. Ji, H. Zhang, Z. L. Sun, L. Kang, B. B. Jin, J. Chen, J. Li, B. Gross, A. Ishii, K. Hirata, T. Hatano, V. P. Koshelets, D. Koelle, R. Kleiner, H. B. Wang, W. W. Xu, and P. H. Wu, Terahertz emission and detection both based on high-T_c superconductors: Towards an integrated receiver, Appl. Phys.Lett. **102**, 092601 (2013).

[71] X. J. Zhou, J. Yuan, H. Wu, Z. S. Gao, M. Ji, D. Y. An, Y. Huang, F. Rudau, R. Wieland, B. Gross, N. Kinev, J. Li, A. Ishii, T. Hatano, V. P. Koshelets, D. Koelle, R. Kleiner, H. B. Wang, and P. H. Wu, Tuning the Terahertz Emission Power of an Intrinsic Josephson-junction Stack with a Focused Laser Beam, Phys. Rev. Applied **3**, 044012 (2015).

[72] H. Eisele, M. Naftaly, and J. R. Fletcher, A simple interferometer for the characterization of sources at terahertz frequencies, Meas. Sci. Technol. **18,** 2623 (2007).

[73] M. Giura, R. Fastampa, S. Sarti, and E. Silva, Normal-state c-axis transport in $Bi_2Sr_2CaCu_2O_{8+\delta}$: Interlayer tunneling and thermally activated dissipation, Phys. Rev. B **68,** 134505 (2003).

[74] T. Watanabe, F. Fujii, and A. Matsuda, Anisotropic Resistivities of Precisely Oxygen Controlled Single-crystal $Bi_2Sr_2CaCu_2O_{8+\delta}$: Systematic Study on "Spin Gap" Effect, Phys. Rev. Lett. **79,** 2113 (1997).

[75] Th. Jacobs, Y. Simsek, Y. Koval, P. Müller, and V. M. Krasnov, Sequence of Quantum Phase Transitions in $Bi_2Sr_2CaCu_2O_{8+\delta}$ Cuprates Revealed by In Situ Electrical Doping of One and the Same Sample, Phys. Rev. Lett. **116,** 067001 (2016).

[76] Compared with Refs. [60,61], in the first term on the right-hand side of Eq. (1) we include the term $\bar{c}^2$ arising from magnetic fields produced by geometric inductances.

[77] In the first term in Eq. (2) we include the scaling with G explicitly, whereas in Refs. [60,61] it was implicitly given in the text.